Tendon force distribution

A key characteristic of tendon-driven systems is the necessity of maintaining positive tendon forces. Indeed, the model is invalid if the tendon tension falls to zero. In such a case, the system does not any longer comply with the equations of motion and may become uncontrollable[1]. Depending on the mechanical design, it might even get damaged. In the Awiwi Hand , the antagonistic configuration and the use of nonlinear springs[2] allows to adjust the joint stiffness by modifying the pretension of the tendons. Therefore, the question arises: How should one select the tendon forces to generate the desired joint torque in real time and realize the desired mechanical stiffness while preventing slackening or overload of the tendons? In the modeling part, it has been shown that the joint torque can be obtained from the tendon forces and the coupling matrix. Therefore, an algorithm that inverses the mapping is needed. However, neither a pseudo-inversion of the coupling matrix nor a projection can guarantee that the desired tendon forces will be restricted to a given range. In the following chapter, the objective is to build an algorithm to set the pretension forces to approximate the user-required mechanical stiffness. Because of the constraints, this is not possible in general and only an approximative solution can be found. First, a formal description of the problem is given. The second section presents several solutions to the problem and discusses the advantages and drawbacks of each method. A pseudo-code that corresponds to the current implementation is reported.

7.1 Problem formulation

As presented in the modeling part, as well as in several works [18, 41], the joint stiffness matrix is obtained by the following transformation

$$\begin{aligned} \boldsymbol{K}_{\mathrm{q}}(\boldsymbol{q}, \boldsymbol{f}_{\mathrm{t}})|_{\boldsymbol{q}=\boldsymbol{q}_0, \boldsymbol{f}_{\mathrm{t}}=\boldsymbol{f}_{\mathrm{t},0}} &= \frac{\partial \boldsymbol{\tau}(\boldsymbol{f}_{\mathrm{t}})}{\partial \boldsymbol{q}}|_{\boldsymbol{q}=\boldsymbol{q}_0, \boldsymbol{f}_{\mathrm{t}}=\boldsymbol{f}_{\mathrm{t},0}} \\ &= \boldsymbol{P}^T(\boldsymbol{q})\frac{\partial \boldsymbol{f}_{\mathrm{t}}}{\partial \boldsymbol{q}} + \frac{\partial \boldsymbol{P}(\boldsymbol{q})^T}{\partial \boldsymbol{q}}|_{\boldsymbol{q}=\boldsymbol{q}_0}\boldsymbol{f}_{\mathrm{t}} \\ &= \boldsymbol{P}^T(\boldsymbol{q})\frac{\partial \boldsymbol{f}_{\mathrm{t}}}{\partial \boldsymbol{h}}\frac{\partial \boldsymbol{h}}{\partial \boldsymbol{q}} + \frac{\partial \boldsymbol{P}(\boldsymbol{q})^T}{\partial \boldsymbol{q}}|_{\boldsymbol{q}=\boldsymbol{q}_0}\boldsymbol{f}_{\mathrm{t}} \\ &= \boldsymbol{P}^T(\boldsymbol{q})\boldsymbol{K}_{\mathrm{t}}(\boldsymbol{f}_{\mathrm{t}})\boldsymbol{P}(\boldsymbol{q}) + \frac{\partial \boldsymbol{P}(\boldsymbol{q})^T}{\partial \boldsymbol{q}}|_{\boldsymbol{q}=\boldsymbol{q}_0}\boldsymbol{f}_{\mathrm{t}} \end{aligned} \quad , \quad (7.1)$$

where $\boldsymbol{P}(\boldsymbol{q}) \in \mathbb{R}^{n\times m}$ is the coupling matrix defined as $\boldsymbol{P}(\boldsymbol{q}) = \partial \boldsymbol{h}(\boldsymbol{q})/\partial \boldsymbol{q}$. $\boldsymbol{q} \in \mathbb{R}^n$ and $\boldsymbol{f}_{\mathrm{t}} \in \mathbb{R}^m$ are the vector of joint angles and the vector of tendon

[1] e. g. due to the change of coupling

[2] The springs themselves are linear but they are used in a mechanism that exhibits a nonlinear stiffness behavior [3].

forces. $\boldsymbol{K}_{\mathrm{t}} = \partial \boldsymbol{f}_{\mathrm{t}} / \partial \boldsymbol{h} \in \mathbb{R}^{m \times m}$ is the tendon stiffness matrix. However, in the Hand Arm System the tendon stiffnesses are independent, thus it is a diagonal matrix. $\boldsymbol{K}_{\mathrm{q}} \in \mathbb{R}^{n \times n}$ is the joint stiffness matrix (positive definite). Classically, $\boldsymbol{q} = \boldsymbol{q}_0, \boldsymbol{f}_{\mathrm{t}} = \boldsymbol{f}_{\mathrm{t},0}$ denote the reference around which the stiffness is calculated. The application that transforms the tendon forces into joint torques and derives the joint stiffness matrix can be defined from (7.1) by

$$\begin{aligned} \Psi: \quad & [f_{\mathrm{t,min}}, f_{\mathrm{t,max}}]^m \mapsto \mathbb{R}^n \times \mathbb{R}^{n \times n} \\ & \boldsymbol{f}_{\mathrm{t}} \to \begin{bmatrix} \boldsymbol{P}(\boldsymbol{q})^T \boldsymbol{f}_{\mathrm{t}} \\ \dfrac{\partial \boldsymbol{P}(\boldsymbol{q})^T}{\partial \boldsymbol{q}} \boldsymbol{f}_{\mathrm{t}} + \boldsymbol{P}^T \boldsymbol{K}_{\mathrm{t}}(\boldsymbol{f}_{\mathrm{t}}) \boldsymbol{P} \end{bmatrix} = \begin{bmatrix} \boldsymbol{\tau} \\ \boldsymbol{K}_{\mathrm{q}} \end{bmatrix} . \end{aligned} \tag{7.2}$$

Therefore, the problem consists in solving the equation

$$\Psi(\boldsymbol{f}_{\mathrm{t}}) = [\boldsymbol{\tau}_{\mathrm{des}}, \boldsymbol{K}_{\mathrm{q,des}}]^T , \quad \text{with} \quad \boldsymbol{f}_{\mathrm{t}} \in [f_{\mathrm{t,min}}, f_{\mathrm{t,max}}]^m , \tag{7.3}$$

where $\boldsymbol{\tau}_{\mathrm{des}} \in \mathbb{R}^4$ is the user-desired torque. The question is to select the tendon forces given a desired joint torque $\boldsymbol{\tau}_{\mathrm{des}}$ and a desired joint stiffness matrix $\boldsymbol{K}_{\mathrm{q,des}}$. The problem is overconstrained since the torque requires four parameters and the symmetric stiffness matrix requires ten parameters, while only eight tendon forces are available.

7.2 Solutions

The problem (7.3) might not accept any solution because of the force range limits. A simple saturation of the solutions to the feasible tendon forces does not ensure that the joint torque is achieved, thus possibly destabilizing the system (the stability proofs are usually not including the nonlinear effects of the force saturation). The desired joint torque must be achieved as closely as possible, possibly even increasing the stiffness error. In order to circumvent this issue the problem is transformed into a quadratic optimization problem under linear constraints.

$$\begin{aligned} & \min_{\boldsymbol{f}_{\mathrm{t}}} (\| \boldsymbol{K}_{\mathrm{q,des}} - \boldsymbol{K}_{\mathrm{q}} \|) \\ & \boldsymbol{\tau}_{\mathrm{des}} = \boldsymbol{P}^T \boldsymbol{f}_{\mathrm{t}} \end{aligned} \quad \text{with} \quad \boldsymbol{f}_{\mathrm{t}} \in [f_{\mathrm{t,min}}, f_{\mathrm{t,max}}]^m , \tag{7.4}$$

where the desired (resp. achieved) joint stiffness matrix is denoted $\boldsymbol{K}_{\mathrm{q,des}} \in \mathbb{R}^{n \times n}$ (resp. $\boldsymbol{K}_{\mathrm{q}} \in \mathbb{R}^{n \times n}$). The norm is the $\mathcal{L}_2$ norm. Because the problem is nonlinear (loosely said: $k_{\mathrm{t}}(\alpha f_{\mathrm{t}}) \neq \alpha k_{\mathrm{t}}(f_{\mathrm{t}})$), it is not possible to separate the selection of the internal tendon forces and the tendon forces that generate a link torque. The non-superposability distinguishes the problem from most of the cases discussed in the literature [53,124]. The transformation that maps the tendon forces in the joint torques and derives the joint stiffness is not bijective in general (but is certainly injective from $[f_{\mathrm{t,min}}, f_{\mathrm{t,max}}]^m$ to $\mathbb{R}^n \times \mathbb{R}^{n \times n}$). Thus, for a given choice of joint stiffness matrix and torque, no exact

solution exists. Moreover, as presented in the tendon modeling chapter, the tendon characteristics are approximated by polynomials or lookup tables. Therefore, it is not possible to explicitly find the inverse function Ψ^{-1} that maps the desired joint torques and stiffness to the tendon forces. It should be noted that the inversion can be reduced to a simple matrix inversion and allows an easier analysis if a suitable tendon stiffness model can be used [54]. A first possible approach to this problem is to perform a nonlinear optimization with constraints defined as,

$$\begin{cases} \min\limits_{\boldsymbol{f}_\mathrm{t}}(\beta_1 \left\|\boldsymbol{K}_\mathrm{q} - \boldsymbol{K}_\mathrm{q,des}\right\| + \beta_2 \left\|\boldsymbol{\tau} - \boldsymbol{\tau}_\mathrm{des}\right\|) \\ \boldsymbol{f}_\mathrm{t} \in [f_\mathrm{t,min} \dots f_\mathrm{t,max}]^m \end{cases}, \tag{7.5}$$

where $(\beta_1, \beta_2) \in \mathbb{R}^2$ are weights to be selected depending on the desired behavior. Unfortunately, this optimization does not ensure that the desired torques are achieved. The stiffness can potentially lead to an incorrect torque and destabilize the system. Due to this stability issue, the torque is more important than the mechanical stiffness. A constraint can be added in the problem to solve the issue,

$$\begin{cases} \min\limits_{\boldsymbol{f}_\mathrm{t}}(\boldsymbol{\beta}_1 \left\|\boldsymbol{K}_\mathrm{q} - \boldsymbol{K}_\mathrm{q,des}\right\|) \\ \boldsymbol{f}_\mathrm{t} \in [f_\mathrm{t,min} \dots f_\mathrm{t,max}]^m \\ \boldsymbol{P}\boldsymbol{f}_\mathrm{t} = \boldsymbol{\tau}_\mathrm{des} \end{cases}, \tag{7.6}$$

where $\boldsymbol{\beta}_1 \in \mathbb{R}^{n\times n}$ is a weight matrix to be selected depending on the relative importance of the joints. This latter formulation revealed to be complex to implement efficiently on the real-time machine, mainly due to the constraints. As a results the solver is not suitable for a real-time use. A reformulation of the problem (inspired by [18]) ensures that the desired torques are achieved if it is possible given the limits of the tendon forces. The problem is given by

$$\min_{\boldsymbol{\alpha}} \left(\gamma_1 \|\boldsymbol{K}_\mathrm{q,des} - \boldsymbol{K}_\mathrm{q}\| + \gamma_2 \Psi(\boldsymbol{f}_\mathrm{t}, \boldsymbol{f}_\mathrm{t,min}) + \gamma_3 \Psi(\boldsymbol{f}_\mathrm{t}, \boldsymbol{f}_\mathrm{t,max})\right), \tag{7.7}$$

where $\boldsymbol{f}_\mathrm{t} = (\boldsymbol{P}^T)^+ \boldsymbol{\tau}_\mathrm{des} + \ker(\boldsymbol{P}^T)\boldsymbol{\alpha}$. The desired joint stiffness matrix (resp. the achieved joint stiffness matrix) is $\boldsymbol{K}_\mathrm{q,des} \in \mathbb{R}^{n\times n}$ (resp. $\boldsymbol{K}_\mathrm{q} \in \mathbb{R}^{n\times n}$). The tendon force limits are $(\boldsymbol{f}_\mathrm{t,min}, \boldsymbol{f}_\mathrm{t,max}) \in \mathbb{R}^2$. The term $\ker(\boldsymbol{P}^T)\boldsymbol{\alpha}$ operates in the null space of the coupling, and therefore, it does not generate any joint torque. The weighting factors γ_1, γ_2, and γ_3 are used to balance the relative importance of the boundary potentials and the error. The boundary function Ψ implements a repulsive potential to repel the solution from the tendon force limits. It is important to note that, in contrast to (7.6) where the search is performed on $\boldsymbol{f}_\mathrm{t} \in \mathbb{R}^m$, in (7.6) the search is performed only on $\boldsymbol{\alpha} \in \mathbb{R}^n$. This reduction of the search space provides a valuable run-time speed-up. Using this formulation, the particular shape of the nullspace of

the coupling matrix is used advantageously to improve the search speed. The pseudo-code corresponding to the search is reported in Alg. 2. The key feature of the algorithm is to ensure that the desired torque is exactly achieved. Although it does not strictly enforce that the force constraints are satisfied, they are in practice achieved since the boundary gains, i. e. γ_2 and γ_3, can be large to prevent the search from exceeding the limits. In particular, this algorithm is extremely efficient with constant coupling matrices (i. e. all fingers but the thumb of the hand of Awiwi Hand). Indeed, if $\boldsymbol{P}$ is constant, a base $\boldsymbol{W}$ of the kernel of $\boldsymbol{P}^T$ can be computed offline. In case of a position-varying coupling matrix, this algorithm needs to compute a singular value decomposition (or a pseudo-inverse) online thus severely impairing its execution time. Nonetheless, in the case of the thumb, despite its position dependance, the special shape of the coupling matrix (block diagonal) allows efficient implementation techniques.

7.3 Discussion

In this chapter, the problem of selecting the internal tendon forces has been described. Since the tendon forces modify the joint stiffness, it is not possible to independently set the stiffness and the torque. Several formulations of the problem are proposed and discussed. Unless assumptions are made on the stiffness function of the tendons, numerical search algorithms are the only available tool to optimally select the tendon forces. Although, initially, the search problem is of dimension equal to the number of tendons, it is possible to restrict the search to a base of the kernel of the coupling matrix. It ensures that the search algorithm satisfies the desired torque and reduces the dimension of the problem. Experimental results have been presented in [41].

Norms In this chapter, the notion of norm is required to define the optimization goals/costs. For real vectors, the norm operation from $\mathbb{R}^n$ to $\mathbb{R}$ defined by (7.8) will be used unless otherwise specified.

$$\|\boldsymbol{x}\| = \sqrt{\sum_{i=0}^{n} x_i^2} \tag{7.8}$$

where $\boldsymbol{x} \in \mathbb{R}^n$ is a real vector of dimension $n \in \mathbb{N}$. $i \in [1 \dots n]$ is a generic summation symbol. For real matrices, the definition is less natural and multiple norms have been proposed (max norm, entrywise norm, Schatten norm, Frobenius norm, [125]). In this chapter, either the norm defined by (7.9) or by (7.10) will be used.

$$\|\boldsymbol{A}\| = \sqrt{\sum_{i=0}^{n} a_i^2} \tag{7.9}$$

or

$$\|\boldsymbol{A}\| = \max a_{i,j} \tag{7.10}$$

where $\boldsymbol{A} \in \mathbb{R}^{n \times n}$ is a real square matrix of dimension $n \in \mathbb{N}$. $(i, j) \in [1 \dots n]^2$ are a generic summation symbols. In most cases, the norms can easily be changed since they are not needed to establish the properties.

Algorithm 2 The projected gradient search algorithm.

% $\boldsymbol{W}$: null space of $\boldsymbol{P}^T$
% s: step size
% $\boldsymbol{g}$: gradient
% ∇: gradient operator
% C: cost at the current point

$\boldsymbol{W} \leftarrow \ker(\boldsymbol{P}^T)$
$\boldsymbol{\alpha} \leftarrow \boldsymbol{\alpha}_0$
$s \leftarrow s_0$
$\boldsymbol{g} \leftarrow 0$
$C_{\text{best}} \leftarrow +\inf$
for $i = 0$ to $\text{N} - 1$ **do**
    $C, \boldsymbol{g} \leftarrow cost_{\boldsymbol{\alpha}}(\boldsymbol{\alpha} - s \cdot \boldsymbol{g})$
    if $C < C_{\text{best}}$ **then**
        $C_{\text{best}} \leftarrow C$
        $\boldsymbol{\alpha} \leftarrow \boldsymbol{\alpha} - s \cdot \boldsymbol{g}$
    else
        $s \leftarrow s/2$
    end if
end for

---

function $cost_{\boldsymbol{\alpha}}(\boldsymbol{\alpha})$
    $\boldsymbol{f}_{\text{t}} \leftarrow (\boldsymbol{P}^T)^{+}\boldsymbol{\tau}_{\text{des}} + \boldsymbol{W}\boldsymbol{\alpha}$
    $C \leftarrow \gamma_1 \|\boldsymbol{K}_{\text{q,des}} - \boldsymbol{K}_{\text{q}}(\boldsymbol{f}_{\text{t}})\| + \gamma_2 \Psi(\boldsymbol{f}_{\text{t}}, \boldsymbol{f}_{\text{t,min}}) +$
        $\gamma_3 \Psi(\boldsymbol{f}_{\text{t}}, \boldsymbol{f}_{\text{t,max}})$
    $\boldsymbol{g} \leftarrow \nabla C$
    return C, $\boldsymbol{g}$
end function

8 Stiffness correction

The fingers of the Awiwi Hand are driven by flexible tendons. As a result of this design, the stiffness obtained at a joint is a combination of the mechanical stiffness and the controller stiffness. In this chapter, two problems are presented. The first problem is the computation of the effective stiffness, that is the stiffness that the user feels. The second problem is the question of generating the controller parameters in order to achieve a given effective stiffness. In the first section, the serial interconnexion of the stiffnesses is modeled. The second section presents a controller that adjusts the stiffness online, in order to yield the user desired stiffness. Several challenges associated with the problem are highlighted. Finally, experiments and simulations confirm the effectiveness of the approach.

8.1 Problem formulation

For a given joint torque, the deflection observed at the joint is generated by three contributions. First, the springs of the tendons are elongated. Then, the motor controller moves the motors according to the impedance control law. In the Awiwi Hand , the motor control is similar to a simple PD controller, therefore the motors do not exactly reach their final position because of the external disturbance. The general case is discussed in [54], however, in the case of the Awiwi Hand , the high position gains of the motors allow to neglect the motor contribution. An alternative consists in adding an integral term to supress the steady-state error. The effective stiffness at the finger joints results from the controller stiffness and the mechanical stiffness. This serial interconnection is expressed by

$$\boldsymbol{K}_{\text{eff}}^{-1} = \boldsymbol{K}_{\text{imp}}^{-1} + \boldsymbol{K}_{\text{mech}}^{-1}, \tag{8.1}$$

where $\boldsymbol{K}_{\text{eff}} \in \mathbb{R}^{n\times n}$(resp. $\boldsymbol{K}_{\text{imp}}^{-1} \in \mathbb{R}^{n\times n}$ and $\boldsymbol{K}_{\text{mech}} \in \mathbb{R}^{n\times n}$) is the effective joint stiffness matrix (resp. the stiffness matrix of the impedance joint controller and the mechanical joint stiffness due to the tendons). This serial interconnection is represented in Figure 8.1. From Equation (8.1) it becomes obvious that by fixing two of the stiffness matrices, it is at least conceptually possible to generate any third matrix.

8.2 Adaptive Controller

The user most likely wants to specify the effective stiffness and does not want to interfere with the rest of the matrices. Therefore, the main concept of this design is to let the user specify an effective link stiffness $\boldsymbol{K}_{\text{eff}}$. Then compute automatically the optimal mechanical stiffness $\boldsymbol{K}_{\text{mech}}$ with respect

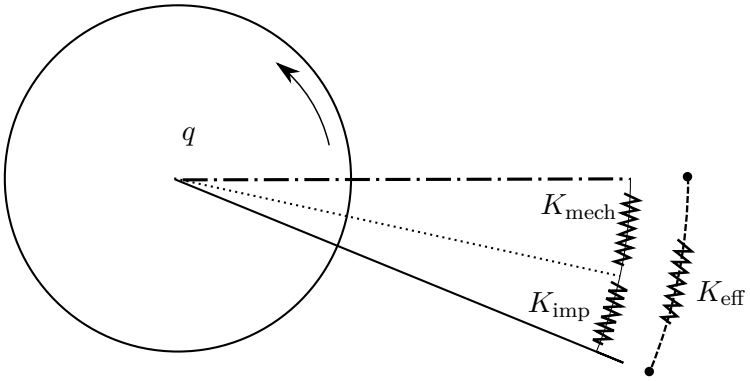

Figure 8.1: Serial interconnexion of the controller stiffness and the mechanical stiffness

to some criteria, such as the maximum robustness or minimum control effort. Finally, the controller impedance gain $\boldsymbol{K}_{\text{imp}}$ is selected to obtain, if possible, the proper effective stiffness. Theoretically, if the adjustment of $\boldsymbol{K}_{\text{imp}}$ is quasi-static, the stability only depends on $\boldsymbol{K}_{\text{eff}}$ being positive definite. It implies that the mechanical stiffness can be arbitrarily selected (but positive definite by nature) and the effective stiffness $\boldsymbol{K}_{\text{eff}}$ can always be achieved. However, it should be noted that non-positive definite gain matrices $\boldsymbol{K}_{\text{imp}}$ are practically often unstable. A non-positive definite matrix corresponds to a *negative* feedback, that is the controller pushes against the disturbance instead of releasing. For the implementation, it is needed to ensure that the gains of the controller remain positive definite, possibly, at the cost of not reaching the desired effective stiffness. The control scheme used to implement this correction is depicted in Fig. 8.2.

8.3 Challenges

In this control scheme, several challenges appear. First, the overall stability of the plant is not guaranteed due to the online adjustment of the impedance gain matrix. Second, if the mechanical stiffness selection algorithm selects a stiffness close to the user-desired effective stiffness, the impedance gains can become infinite ($\boldsymbol{K}_{\text{eff}}^{-1} = \boldsymbol{K}_{\text{mech}}^{-1} \rightarrow \boldsymbol{K}_{\text{imp}}^{-1} = \boldsymbol{0}$). Therefore, the implementation must prevent such a case and rules should be devised for the mechanical stiffness selection to circumvent this issue.

The stability question is challenging, involving a nonlinear adaptive controller for a nonlinear plant. A possible solution consists in building a controller that ensures that the plant remains passive [126]. It is an approach mostly used in telemanipulation scenarios. Despite its implementation simplicity, the method requires to estimate the energy dissipation in the system which is a delicate task.

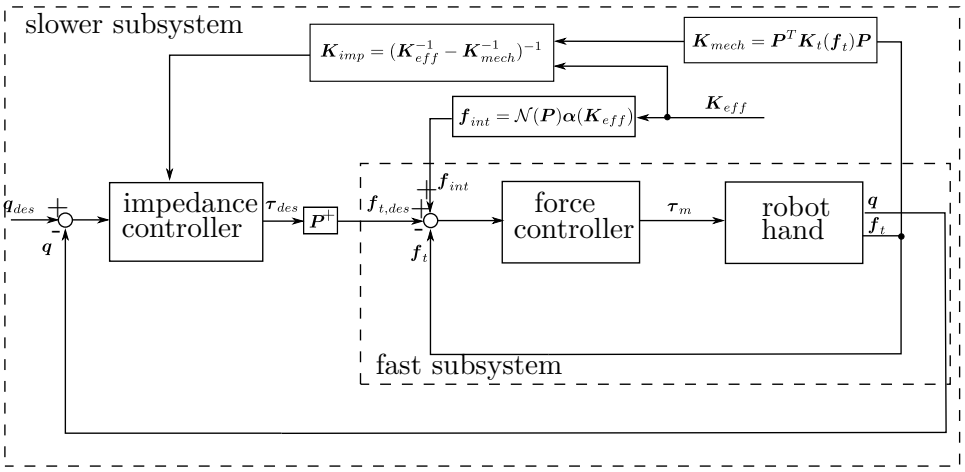

Figure 8.2: Control structure used for adjusting online the impedance gain to obtain the desired effective impedance.

The second question, that is the selection of the controller parameters to achieve the user-desired effective stiffness, can be answered in several ways. A simple and practical solution consists in selecting a mechanical stiffness always higher than the desired, therefore avoiding the asymptotic cases. Such a selection can be,

$$\boldsymbol{K}_{\text{mech,des}} = \epsilon \boldsymbol{K}_{\text{eff,des}}, \tag{8.2}$$

where $\epsilon > 1 \in \mathbb{R}$ is a positive constant used to avoid the singular cases (practically 2 or 3 are good values). The desired mechanical stiffness matrix (resp. the desired effective stiffness matrix) is denoted $\boldsymbol{K}_{\text{mech,des}} \in \mathbb{R}^{n \times n}$ (resp. $\boldsymbol{K}_{\text{eff,des}} \in \mathbb{R}^{n \times n}$). A more involved answer consists in designing both gains $(\boldsymbol{K}_{\text{imp}}, \boldsymbol{K}_{\text{mech}})$ in an optimal manner with respect to a cost function that integrates the asymptotic issue. For example, the gains could be selected according to some weights on the robustness and the accuracy. An open research problem is the question of the choice of the mechanical stiffness that would minimize the controller action. Indeed, selecting the closest mechanical stiffnesses for some joints, is not necessarily minimizing the effort needed to achieve the other directions. Moreover, recent work on the arm control showed that it is possible to achieve limit cycles if the joint stiffness is selected properly. The stability of a grasp can also be improved by choosing suitable joint stiffnesses such that the internal forces are primarily maintained by the springs thus easing the controller task.

8.4 Simulation and experiments

Selecting the target mechanical stiffness 1.5 times the value of the effective stiffness shows acceptable results. The measurements reported in Figure

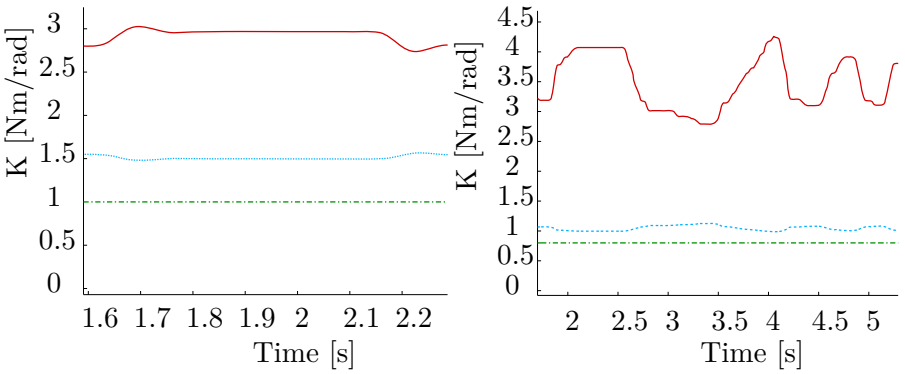

(a) Simulation (b) Experiment

Figure 8.3: Effective stiffness using the active correction. The red/solid curve depicts the impedance controller stiffness. The blue/dotted curve represents the mechanical stiffness. The green/dashed dotted curve depicts the resulting, nearly constant, stiffness.

8.3a are obtained on a single joint using a simulation model that includes the calibration curve and a structure identical to the control model (only the hardware block is replaced by a plant model). Figure 8.3b reports the real system measurements. In both cases the green/dashed-dotted line depicts the effective stiffness $\boldsymbol{K}_{\text{eff}}$ computed according to (8.1). The red/solid curve shows the impedance gain $\boldsymbol{K}_{\text{imp}}$ and the light blue/dotted curve represents the mechanical stiffness $\boldsymbol{K}_{\text{mech}}$ (estimated from the desired tendon forces to limit the noise). The perturbations in the simulation and the experiment are generated by applying a disturbance to the link. It can be seen that the effective stiffness is regulated around its desired value (1 Nm/rad and 0.7Nm/rad) although the external disturbances modify the mechanical stiffness.

8.5 Discussion

The method performs as expected but its effect is not noticeable during the experiments. Indeed, it is very difficult for a human user to evaluate the stiffness of a fingertip mainly due to other effects such as the joint friction. Therefore, this stiffness compensation scheme is not used in the following work since its advantages are limited and it lacks a stability proof. More experimental results and details are presented in [55]. Nonetheless, the method shows that it is possible to select the stiffness matrices in order to generate a constant effective stiffness. There might exist a choice of stiffness that optimizes the robustness (the spring storage is fully available) or the precision since the sensitivity to disturbances decreases with the stiffness.

However, the joint friction increases with the stiffness, therefore it seems intuitive that there exists an optimal choice of the mechanical stiffness, e. g. to maximize robustness. It is part of future works to study the trade-off between robustness and accuracy. Eventually, the robot could modulate the internal forces to adapt to its task, such as precision manipulation or tactile exploration.

9 Joint torque observer

As presented in the tendon modeling chapter, the tendon friction due to the pulleys and the sliding surfaces creates a substantial error in the tendon force estimation. Depending on the mounting condition and the routing path, the tendon friction reaches 10 % to 50 %. That is for a measured force of 20 N the effective pulling force is between 10 N and 30 N. Consequently, even an ideal control scheme cannot produce the desired behavior (a deflection of the link is not corrected even without any external disturbance because the estimated joint torque is biased). For the mechanical designers it is important to understand the influence of the tendon friction. According to the desired performance, the materials or the routing might be revised possibly at the expense of reduced maximum torque. To bring more sensitivity to the finger, an external force sensor can be used to circumvent the tendon friction error. Similar to other hands developed at the institute, some strain gauges have been placed on the bone of the finger. This has been done mostly for testing purposes since the introduction of sensors and cables in the fingers jeopardizes the robustness of the complete system. Indeed, if applied to the complete system, around 100 tiny cables would be required between the strain gauges and the analog converters. Therefore, the work of this chapter is carried out to obtain an idea of the system capabilities, if the measurements of the tendon forces perfectly represented the joint torques.

The first section briefly describes the structure of the controller and explains the main ideas. The details about the stability and the passivity aspects of the controller are found in [58]. The second section presents simulations, the implementation and experimental results.

9.1 Structure

The friction compensation mechanism is based on the idea of estimating the external joint torque by comparing the model dynamics and the observed dynamics. It is similar to the collision detection algorithm presented in [127]. The observer compares the applied torque and the measured acceleration and identifies the missing part to the friction. The actuator dynamics is

$$u = B\ddot{\theta} + \tau + \tau_{\text{fric}}\,, \tag{9.1}$$

where $u \in \mathbb{R}$ is the applied motor torque, $\ddot{\theta} \in \mathbb{R}$ is the motor acceleration. $B \in \mathbb{R}$ is the motor inertia around the rotation axis and $\tau \in \mathbb{R}$ (resp. $\tau_{\text{fric}} \in \mathbb{R}$) is the joint torque (resp. the friction torque). As depicted in Fig. 9.1, the observer equations are

$$\begin{aligned} u = &\quad B\ddot{\hat{\theta}} + \tau_a + \hat{\tau}_{\text{fric}} \\ \hat{\tau}_{\text{fric}} = &\quad -LB(\dot{\theta} - \dot{\hat{\theta}}) \end{aligned}\,, \tag{9.2}$$

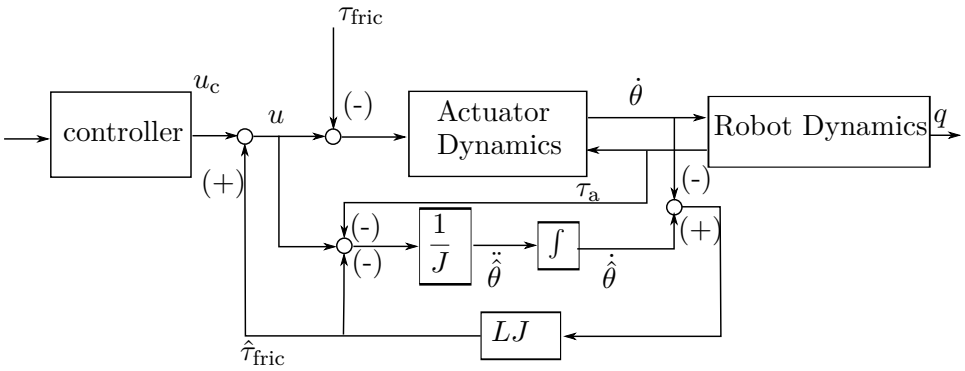

Figure 9.1: Structure of the link side friction observer

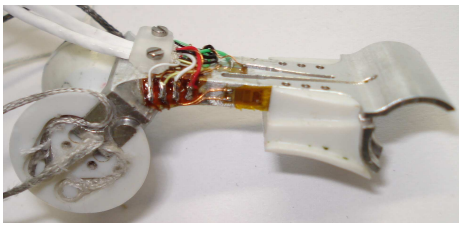

(a) Picture of the real strain gauges in the finger base

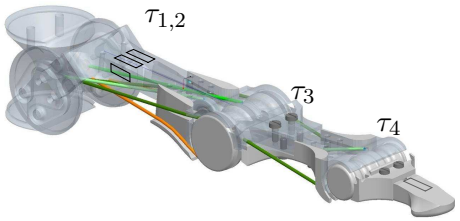

(b) Placement of the strain gauges (in hatched black)

Figure 9.2: Placement of the stain gauges in the index finger

where $L \in \mathbb{R}^+$ is an observer gain to be selected. The structure of (9.2) is the one of a Luenberger observer [128]. Finally, the control input is modified as $u = u_c + \hat{\tau}_{\text{fric}}$, which effectively compensates for the estimated friction torque. As mentioned in [58], the friction observer results in a filtered version of the real friction. Thus, the design is not always passive and might, at least for a short period of time, input more energy than needed. The analysis provided in [58] shows that the passivity mainly depends on the friction model.

9.2 Experimental setup

The experiments are conducted on the index finger of the right hand. In order to implement the controller described above, a direct access to the joint torque is required. To that end, eight strain gauges are applied directly to the structure of the finger (namely the bones). A total of four degrees of freedom are measured, two for the base (cf. Fig. 9.2a), one for the PIP and one for the DIP (cf. Fig. 9.2b). The observer is implemented for the complete finger but only the PIP results are presented for brevity.

9.3 Simulation and experiments

A slow sinusoidal motion profile for the link side is used for the evaluation of the observer. Four cases are studied:

1. Simulation without compensation (cf. Fig. 9.3a).
2. Simulation with compensation (cf. Fig. 9.3b).
3. Experiment without compensation (cf. Fig. 9.3c).
4. Experiment with compensation (cf. Fig. 9.3d).

The improvements, due to the use of the link side measurement, that are visible in the simulations (cf. Fig. 9.3a and Fig. 9.3b) are clearly visible in the experiments (cf. Fig. 9.3c and Fig. 9.3d). The simulations are performed with low stiffness and link damping to highlight the improvements.

9.4 Discussion

The joint friction observer presented in this section proved that a reduction of the joint friction significantly improves the tracking performance. However, it is important to mention that the compensation leads to a violent reaction of motors. Indeed, around a given position, the estimation of the stick slip results in a bang bang style estimation. Moreover, around the equilibrium the stiffness is minimal, emphasizing the required motion of the motors (for the same change of torque the motion of the motors is inversely proportional to the stiffness). More results on the fingers are reported in [129] as well as tests with different tendon materials and different finger configurations. To obtain long term results, the joint friction should be reduced mechanically. Indeed, a reduction of the mechanical friction is expected to lead to a positioning accuracy similar to the one obtained with the joint torque observer but without the chattering effect.

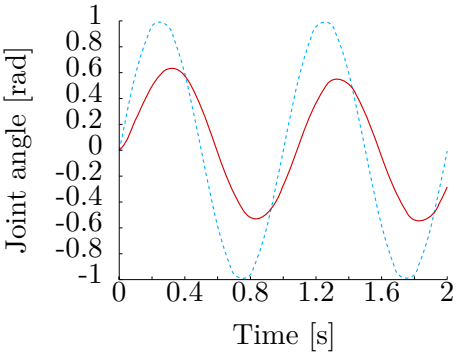

(a) Simulation: Joint position without compensation

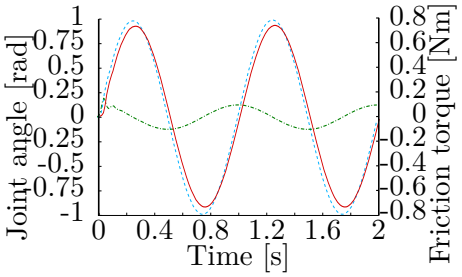

(b) Simulation: Joint position with compensation

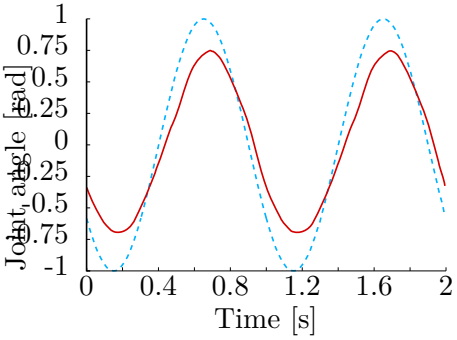

(c) Experiment: Joint position without compensation

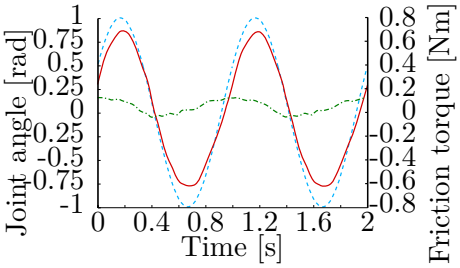

(d) Experiment: Joint position with compensation

Figure 9.3: Joint tracking performance in simulation (top) and in experiments (bottom). A sinusoidal trajectory, represented in light blue/dotted is used as reference joint trajectory. The effective joint motion is represented in red/solid. The estimated joint friction torque is depicted by the green/dashed-dotted curve.

10 Tendon control

This chapter describes the control of the tendon forces. The control of the tendon forces is needed to implement the cascaded control and its performance gives a good insight in the best performance that could be achieved. It also helps to understand the effect of the nonlinear springs and to verify the validity of the modeling. First, a tendon force dynamic model is described that consists of a motor, a spring element, and a tendon. In the second section a force controller is designed. The feedforward term is added to significantly reduce the steady-state error. However, because the controller gains are selected for a specific working point, the controller is not adapted to the complete workspace. Therefore, in the third section, a gain scheduling controller is derived in order to deal with the changing stiffness. It is simulated on a plant similar to the real one in terms of noise and quantization and exhibits the desired behavior. Finally, experiments are performed to verify the applicability of the method on the real system.

10.1 Control model

According to the modeling part, the motor/tendon subsystem is modeled as a second order system. The equation of dynamics, reported for ease of reference, is

$$B\ddot{\theta} = \tau_{\text{fric}}(\theta, \dot{\theta}) + \tau_{\text{m}} + \tau_{\text{f}_\text{t}} \ , \tag{10.1}$$

where $B \in \mathbb{R}$ is the motor inertia, $\theta \in \mathbb{R}$ (resp. $\dot{\theta} \in \mathbb{R}, \ddot{\theta} \in \mathbb{R}$) is the motor position (resp. velocity, acceleration). The torque resulting for the viscous and static friction is denoted $\tau_{\text{fric}}(\theta, \dot{\theta}) \in \mathbb{R}$. The motor torque is denoted $\tau_{\text{m}} \in \mathbb{R}$. The torque generated by the tendon force is denoted by $\tau_{\text{f}_\text{t}} = r f_{\text{t}}(\theta)$, where $r \in \mathbb{R}$ and $f_{\text{t}} \in \mathbb{R}$ are the motor pulley radius and the tendon force. The dynamics are nonlinear because the function $f_{\text{t}}(\theta)$ is not linear in its arguments. This nonlinear behavior is the very reason why it is not possible to directly use linear design methods.

10.2 Controller design

A PD controller is used for the tendon force control. The control law is

$$\boldsymbol{\tau}_{\text{m}} = K_{\text{p}}(f_{\text{t,des}} - f_{\text{t}}) + K_{\text{d}}(\dot{f}_{\text{t,des}} - \dot{f}_{\text{t}}) + \hat{\tau}_{\text{fric}}(\theta, \dot{\theta}) + \hat{\tau}_{\text{f}_\text{t}} \ , \tag{10.2}$$

where $(K_{\text{p}}, K_{\text{d}}) \in \mathbb{R}^2$ are positive gains and $\hat{(\cdot)}$ denotes an estimated quantity. The desired tendon force and the velocity of the desired tendon force are denoted $f_{\text{t,des}} \in \mathbb{R}$ and $\dot{f}_{\text{t,des}} \in \mathbb{R}$. A friction compensation and a torque feedback term are used in order to shorten the rise time and reduce the

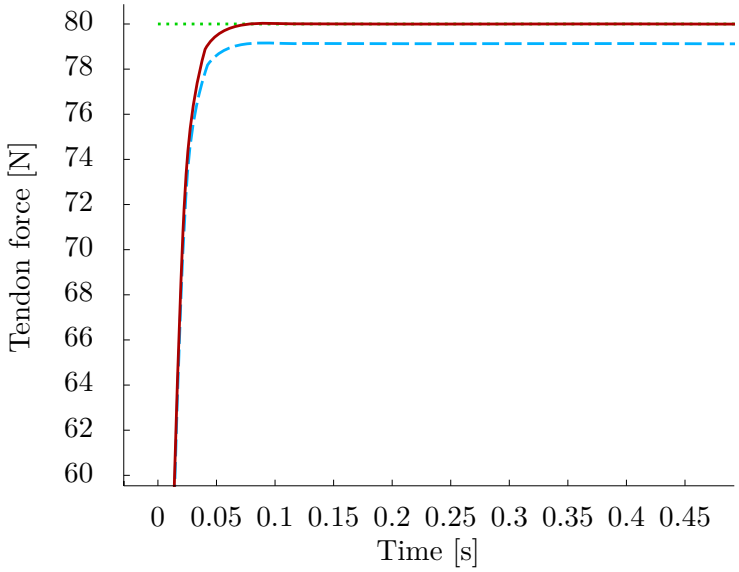

Figure 10.1: Simulation: force step response of the plant with and without feedforward terms. The dotted/green curve denotes the desired force. The blue/dashed curve represents the force without feedforward term. The solid/red curve represents the force with feedforward term.

steady-state error. Figure 10.1 depicts that the steady-state error is reduced by the feedforward terms. It is important to note that the improvements visible in the experiments are smaller than in simulations because of the imprecision of the models and the impossibility to achieve perfect measurements. The steady-state error is obtained by setting all time derivatives to zero in Eq. (10.2). Without feedforward term, the error is

$$f_{\mathrm{t,des}} - f_{\mathrm{t}} = -\frac{1}{K_{\mathrm{p}}}\left(\tau_{\mathrm{fric}}(\theta,\dot{\theta}) + \tau_{\mathrm{f_t}}\right) \ , \tag{10.3}$$

whereas, with compensation, the error is

$$f_{\mathrm{t,des}} - f_{\mathrm{t}} = \frac{1}{K_p}\left(\tau_{\mathrm{fric}}(\theta,\dot{\theta}) - \hat{\tau}_{\mathrm{fric}}(\theta,\dot{\theta}) + \tau_{\mathrm{f_t}} - \hat{\tau}_{\mathrm{f_t}}\right) \ , \tag{10.4}$$

which, if the observer is properly designed, is smaller since $\|\tau_{\mathrm{fric}}(\theta,\dot{\theta}) + \tau_{\mathrm{f_t}} - \hat{\tau}_{\mathrm{fric}}(\theta,\dot{\theta}) - \hat{\tau}_{\mathrm{f_t}}\| < \|\tau_{\mathrm{fric}}(\theta,\dot{\theta}) + \tau_{\mathrm{f_t}}\|$. If the observer of the estimates is asymptotically stable (that is $\lim_{t\to\mathrm{inf}}(\hat{\tau}_{\mathrm{fric}}(\theta,\dot{\theta})) = \tau_{\mathrm{fric}}(\theta,\dot{\theta})$ and $\lim_{t\to\mathrm{inf}}(\hat{\tau}_{\mathrm{f_t}}) = \tau_{\mathrm{f_t}}$), the regulation is perfectly achieved with respect to the modeling assumptions. Under the assumption that the estimation errors are negligible the closed-loop equation, obtained by combining Eq. (10.1) and Eq. (10.2), is

$$B\ddot{\theta} = K_{\mathrm{p}}(f_{\mathrm{t,des}} - f_{\mathrm{t}}) + K_{\mathrm{d}}(\dot{f}_{\mathrm{t,des}} - \dot{f}_{\mathrm{t}}) \ . \tag{10.5}$$

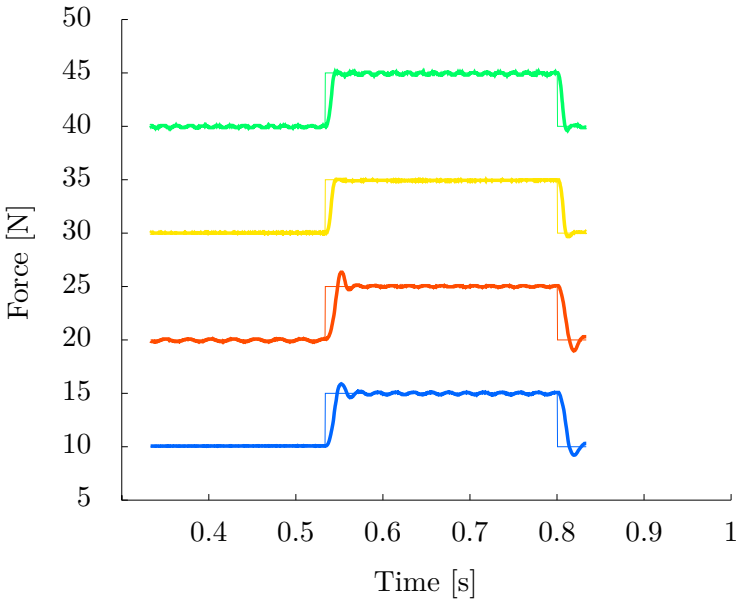

Figure 10.2: Force step response of the controller whose gains are tuned for 30 N. The gains are tuned to obtain the fastest settling time without overshoot. In each experiment, only the initial tendon force and the target tendon force are modified. It can be observed that the response is ideal for 30 N but underdamped for 10 N and 20 N.

It is possible to adjust the controller gains manually to obtain a satisfying behavior since there are only two parameters to tune. However, since θ and f_t are not linearly dependent, the closed loop equation is neither linear in the motor position nor in the tendon force. Therefore, a fixed gain tuning is limited to the vicinity of a force reference. In Figure 10.2, several step responses for a controller tuned for critical damping at 30 N are reported. As expected, it is not well adapted for the other working points. The controller is underdamped if the tendon stiffness is lower than expected (e. g. 20 N). If the stiffness is higher than expected, the controller is underdamped and its rise time could be reduced (up to the saturation of the motor torque). The steady state is obtained by setting all time derivatives to zero in (10.5). If $f_\mathrm{t}(\theta)$ is bijective, the equilibrium is unique and given by $\theta_\mathrm{eq} = f_\mathrm{t}^{-1}(f_\mathrm{t,des})$. Practically, the function f is continuous and strictly increasing on the interval $[f_\mathrm{t,min}, f_\mathrm{t,max}]$ and therefore is a bijection. Although the steady-state force is the desired one, it is important to note that the gains of the system cannot be directly selected by identification to a second order system since the closed-loop equation is not linear in the controlled variable f_t. The objective is to regulate the tendon force to a reference and specify the transient behavior of the tendon force (or the motor position) and not to deal with a combination of both variables. Therefore, in the following sections, this

simple controller is improved to fit the different working points and to allow to specify the transient behavior in terms of f_t or θ.

10.3 Gains scheduling design

The basic concept of the gain scheduling method consists in selecting the gains adapted to each working point, in order to improve the performance of the controller described by (10.2). The first step of the method requires to express the dynamics in terms of a scheduling variable. Then, the controller gains are selected under the assumption that the scheduling variable is frozen and a table of parameters is constructed (or an analytic expression when possible). Finally, for the current scheduling variable, the controller gains are extracted from the table (or evaluated from the analytic expression). Numerous methods to *interpolate* the gains have been proposed that fit the specific meaning of the scheduling variable (e. g. piecewise continuous, linear interpolation). In the tendon control case, the regularity of the stiffness function leads to the choice of a simple linear interpolation. The gain scheduling method is very powerful in the sense that it can be applied to a very large variety of nonlinear problems by linearization. However, it is not generally ensuring the global asymptotic stability.

10.3.1 Linearized form

The first step needed to apply the gain scheduling method consists in writing the dynamics to make the scheduling variable appear. The scheduled form is obtained by linearizing the dynamics around a working point but the choice of the linearization variable is free. In the present case, the linearization is done w. r. t. the tendon force or the motor position which are the most natural coordinates of the problem. It should be noted that in general, a partial feedback linearization does not enforce a particular choice of coordinates. It allows to work with the coordinates that are the most explicit to the designer, at the expense of a feedback to cancel the extra terms. The case of linearization w. r. t. the motor position θ is reported here, the case of the tendon force can be derived in a similar way. The tendon force function is assumed to be sufficiently smooth. Around a point $\theta_\mathrm{des} \in \mathbb{R}$ selected such that $f_\mathrm{t}(\theta_\mathrm{des}) = f_\mathrm{des}$, the force and the time derivate of the force are expressed by

$$f_\mathrm{t}(\theta_\mathrm{des} + \delta\theta) = f_\mathrm{t}(\theta_\mathrm{des}) + \frac{\partial f_\mathrm{t}}{\partial \theta}|_{\theta_\mathrm{des}} \delta\theta, \tag{10.6}$$

$$\dot{f}_\mathrm{t}(\theta_\mathrm{des}+\delta\theta, \dot{\theta}_\mathrm{des}+\delta\dot{\theta}) = \dot{f}_\mathrm{t}(\theta_\mathrm{des}, \dot{\theta}_\mathrm{des}) + \frac{\partial \dot{f}_\mathrm{t}}{\partial \theta}|_{\theta_\mathrm{des},\dot{\theta}_\mathrm{des}} \delta\theta + \frac{\partial \dot{f}_\mathrm{t}}{\partial \dot{\theta}}|_{\theta_\mathrm{des},\dot{\theta}_\mathrm{des}} \delta\dot{\theta}\ , \tag{10.7}$$

where $\delta\theta \in \mathbb{R}$ represents an infinitesimal change of the motor position θ. Defining $\alpha = \partial f_\mathrm{t}/\partial\theta|_{\theta_\mathrm{des}}$, $\beta = \partial \dot{f}_\mathrm{t}/\partial\theta|_{\theta_\mathrm{des},\dot{\theta}_\mathrm{des}}$ and $\gamma = \partial \dot{f}_\mathrm{t}/\partial\dot{\theta}|_{\theta_\mathrm{des},\dot{\theta}_\mathrm{des}}$ yields

$$B(\ddot{\theta}_\mathrm{des} + \ddot{\delta}\theta) = K_\mathrm{p}(f_\mathrm{t,des} - (f_\mathrm{t}(\theta_\mathrm{des}) + \alpha\delta\theta)) + K_\mathrm{d}(\dot{f}_\mathrm{t,des} - (\dot{f}_\mathrm{t}(\theta_\mathrm{des}) + \beta\dot{\delta\theta}))) \ , \tag{10.8}$$

which is a linear differential equation in $\delta\theta$ with the scheduling variables α and β.

10.3.2 Fixed gain controller design

Using the linearized closed-loop defined by (10.8), the gains $(K_\mathrm{p}, K_\mathrm{d}) \in \mathbb{R}^2$ can be selected to obtain the desired behavior. Since, by definition, $f_\mathrm{t}(\theta_\mathrm{des}) = f_\mathrm{t,des}$, (10.12) can be simplified to

$$\ddot{\delta}\theta + \frac{K_\mathrm{d}}{B}\beta\dot{\delta\theta} + \frac{K_\mathrm{p}}{B}\alpha\delta\theta = \frac{1}{B}(\ddot{\theta}_\mathrm{des} + K_\mathrm{d}(\dot{f}_\mathrm{t,des} - \dot{f}_\mathrm{t}(\theta_\mathrm{des}))) \ . \tag{10.9}$$

The gains are selected by identification to obtain the target closed-loop dynamics that is a damped second order system for the error dynamics $\delta\theta$. The right hand side of Eq. (10.9) is independent of time, thus it is possible to identify the desired gains, which yields the system

$$\begin{aligned} \omega^2 &= \frac{K_\mathrm{p}}{B}\beta \\ 2\xi\omega &= \frac{K_\mathrm{d}}{B}\alpha \end{aligned} \ , \tag{10.10}$$

where $\omega \in \mathbb{R}$ is the desired angular frequency and $\xi \in \mathbb{R}$ the desired damping ratio. Solving the system of (10.10), leads to

$$\begin{aligned} K_\mathrm{p} &= \frac{\omega^2 B}{\beta} \\ K_\mathrm{d} &= \frac{2\xi\omega B}{\alpha} \end{aligned} \ . \tag{10.11}$$

As one might expect, the gains are properly defined only if $\alpha > 0$ and $\beta > 0$. This condition expresses that the system should not be degenerated in order to place the poles. Indeed, it is not possible to place the poles of a system where the stiffness vanishes since, in such a case, the tendon force and the motor are not related anymore. The issue is well known by the mechanical designers and the stiffness in the Awiwi Hand is never equal to zero. The case of a vanishing stiffness involves, for example, the use of hysteresis or dead-zone functions but is not treated in the work.

10.3.3 Gain scheduled controller

As pointed out in [84, p.488], the model resulting from the linearization of the system with the fixed gain controller and the model resulting from the linearization of the system with scheduled gains are not equal. In both cases, the desired steady state is the equilibrium, however, the transfer functions are different. Depending on the control objective, the controller design can be acceptable or can be modified to yield the desired transfer function. It is considered acceptable for the Hand Arm System to have a different transfer function since, experimentally, the transfer function is qualitatively close enough to the desired one. The linearized closed-loop equation under the action of the fixed gain controller is obtained by substituting the gains of (10.11) into (10.5) and gives

$$\ddot{\delta\theta} + 2\xi\omega\dot{\delta\theta} + \omega^2\delta\theta = \frac{1}{B}(\ddot{\theta}_0 + K_{\mathrm{d}}(\dot{f}_{\mathrm{t,des}} - \dot{f}_{\mathrm{t}}(\theta_0))). \tag{10.12}$$

Around any constant desired working point (i. e. in the regulation case), the right hand side vanishes and the error dynamics is indeed the one of a linear second order differential equation with the selected poles.

10.4 Experimental and simulation results

The gain scheduling method proposed in the previous section is simulated on a single tendon. The model uses the friction and ripple models developed in the Chapter 3. The stiffness characteristics of a calibrated tendon are used to provide a realistic force/stiffness displacement curve. Noise of an amplitude similar to the one observed on the real system is added through a sensor model (quantization and white noise). The test pattern consists of a force step from 10N (resp. 20N, 30N and 40N) to a force of 20N (resp. 30N, 40N and 50N) and is repeated several times. The test pattern is used in four different cases:

1. Simulation with fixed gains (cf. 10.3a).
2. Simulation with scheduled gains (cf. 10.3b).
3. Experiment with fixed gains (cf. 10.4a).
4. Experiment with scheduled gains (cf. 10.4b).

The simulations and the experiments both confirm that the method is successful. The transient behavior of the force, that was underdamped or overdamped under the fixed gain controller, is always well damped under the scheduled gain controller. Although only approximative (the partial derivative of the gains modifies the pole locations), the method is intuitive and relatively easy to implement. A more detailed experimental work which

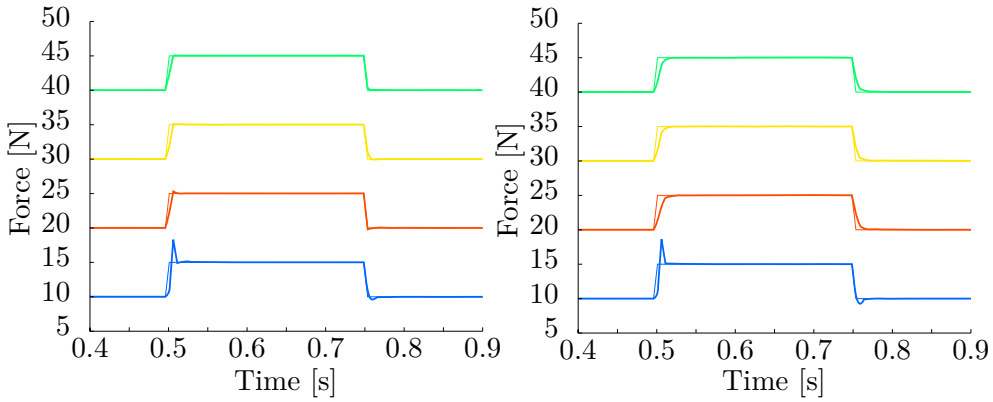

(a) Simulation: Fixed gains (b) Simulation: Adaptive gains

Figure 10.3: Simulations: Tendon force control with/without adaptive gains. In both figures, the measured and desired tendon force is depicted. A step of 5N is commanded from different initial states. The adaptive controller is superior to the fixed gain controller except for the lowest force which is due to the saturation of the control input. The fixed gain controller is tuned for 30N.

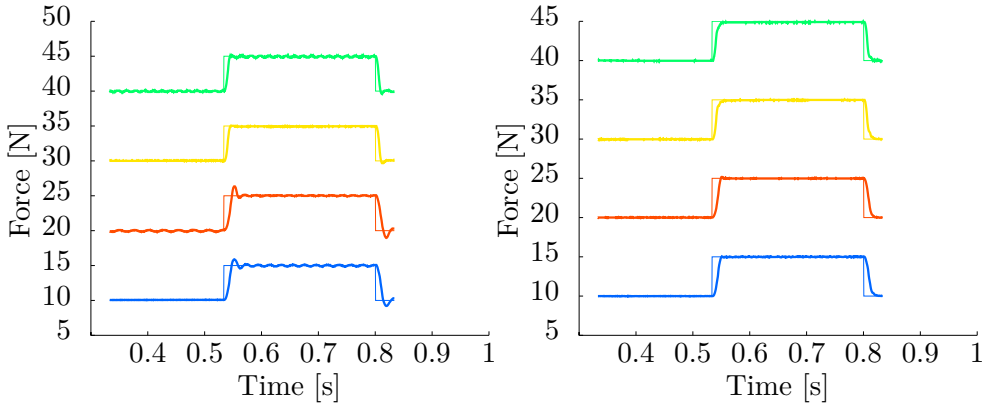

(a) Experiments: Fixed gains (b) Experiments: Adaptive gains

Figure 10.4: Experiments: Tendon force control with/without adaptive gains. In both figures, the measured and desired tendon force is depicted. A step of 5N is commanded from different initial states. The adaptive controller is superior to the fixed gain controller for all the cases. The fixed gain controller is tuned for 30N.

is not reported here, shows that the scheduling in β can be neglected and only α has a noticeable influence. Unsurprisingly, α is nothing else but the tendon stiffness (up to a multiplicative constant) at each working point.

10.5 Discussion

In this chapter, a tendon force controller is presented. A proportional derivative controller for the tendon force using fixed gains is implemented and experiments have been conducted. However, since the system is nonlinear, the controller gains can only be tuned for a specific working point and the controller is underdamped or overdamped around the nominal point. The experimental results and the simulations both confirm it. The linearization of the state dynamics allows to use a gain scheduling method that adapts the gains at each working point. The use of state dependent gains enables to design the gains by identification and to set directly the poles of a linear differential equation of the motor position error. The method only requires the derivative of the stiffness curve. Experiments and simulations confirm that the controller is indeed well damped for all the working points. It should be noted, however, that vibrations appear at higher stiffness mostly due to the noise introduced by the high derivatives. A limitation of the gain design is the fact that it does not account for the control input magnitude (as with all linearization or pole placement methods). Therefore, the controller should be tested on the complete working range to ensure that nonlinear effects of an input saturation are not destabilizing the plant. Indeed, at low stiffness, the control effort is not very effective and a large motor displacement is needed for a small force adjustment.